Mid-infrared supercontinuum generation in As_2S_3-silica "nano-spike" step-index waveguide

N. Granzow, M. A. Schmidt, W. Chang, L. Wang, Quentin Coulombier, J. Troles, P. Toupin, I. Hartl, K. F. Lee, M. E. Fermann, et al.

Mid-infrared supercontinuum generation in As_2S_3-silica "nano-spike" step-index waveguide

N. Granzow,[1,*] M. A. Schmidt,[1,7] W. Chang,[1] L. Wang,[1] Q. Coulombier,[2] J. Troles,[3] P. Toupin,[3] I. Hartl,[4] K. F. Lee,[4] M. E. Fermann,[4] L. Wondraczek[5] and P. St.J. Russell[1,6]

[1]*Max Planck Institute for the Science of Light, Guenther-Scharowsky Str. 1, 91058 Erlangen, Germany*
[2]*Université Lille 1, Laboratoire PhLAM UMR8523, 59658 Villeneuve d'Ascq Cedex, France*
[3]*Université de Rennes I, Sciences Chimiques de Rennes, 35042 Rennes, France*
[4]*IMRA America, Inc., Ann Arbor, MI 48105, USA*
[5]*Otto-Schott-Institute, University of Jena, 07743 Jena, Germany*
[6]*Department of Physics, University of Erlangen-Nuremberg, 91058 Erlangen, Germany*
[7]*Institute of Photonic Technology, Albert-Einstein-Str. 9, 07745 Jena, Germany*
[*]*nicolai.granzow@mpl.mpg.de*
www.pcfiber.com

Abstract: Efficient generation of a broad-band mid-infrared supercontinuum spectrum is reported in an arsenic trisulphide waveguide embedded in silica. A chalcogenide "nano-spike", designed to transform the incident light adiabatically into the fundamental mode of a 2-mm-long uniform section 1 μm in diameter, is used to achieve high launch efficiencies. The nano-spike is fully encapsulated in a fused silica cladding, protecting it from the environment. Nano-spikes provide a convenient means of launching light into sub-wavelength scale waveguides. Ultrashort (65 fs, repetition rate 100 MHz) pulses at wavelength 2 μm, delivered from a Tm-doped fiber laser, are launched with an efficiency ~12% into the sub-wavelength chalcogenide waveguide. Soliton fission and dispersive wave generation along the uniform section result in spectral broadening out to almost 4 μm for launched energies of only 18 pJ. The spectrum generated will have immediate uses in metrology and infrared spectroscopy.

OCIS codes: (060.2280) Fiber design and fabrication; (060.2390) Fiber optics, infrared; (060.4370) Nonlinear optics, fibers; (060.7140) Ultrafast processes in fibers; (320.6629) Supercontinuum generation.

References and links

1. J. S. Y. Chen, T. G. Euser, N. J. Farrer, P. J. Sadler, M. Scharrer, and P. St. J. Russell, "Photochemistry in photonic Crystal Fiber Nanoreactors," Chemistry **16**(19), 5607–5612 (2010).
2. C. F. Kaminski, R. S. Watt, A. D. Elder, J. H. Frank, and J. Hult, "Supercontinuum radiation for applications in chemical sensing and microscopy," Appl. Phys. B **92**(3), 367–378 (2008).
3. J. H. Frank, A. D. Elder, J. Swartling, A. R. Venkitaraman, A. D. Jeyasekharan, and C. F. Kaminski, "A white light confocal microscope for spectrally resolved multidimensional imaging," J. Microsc. **227**(3), 203–215 (2007).
4. H. Kano and H. O. Hamaguchi, "In-vivo multi-nonlinear optical imaging of a living cell using a supercontinuum light source generated from a photonic crystal fiber," Opt. Express **14**(7), 2798–2804 (2006).
5. C. H. Li, A. G. Glenday, A. J. Benedick, G. Q. Chang, L. J. Chen, C. Cramer, P. Fendel, G. Furesz, F. X. Kärtner, S. Korzennik, D. F. Phillips, D. Sasselov, A. Szentgyorgyi, and R. L. Walsworth, "In-situ determination of astro-comb calibrator lines to better than 10 cm^{-1}," Opt. Express **18**(12), 13239–13249 (2010).
6. T. Udem, R. Holzwarth, and T. W. Hänsch, "Optical frequency metrology," Nature **416**(6877), 233–237 (2002).
7. I. Hartl, X. D. Li, C. Chudoba, R. K. Ghanta, T. H. Ko, J. G. Fujimoto, J. K. Ranka, and R. S. Windeler, "Ultrahigh-resolution optical coherence tomography using continuum generation in an air-silica microstructure optical fiber," Opt. Lett. **26**(9), 608–610 (2001).
8. G. Humbert, W. J. Wadsworth, S. Leon-Saval, J. C. Knight, T. Birks, P. St J Russell, M. Lederer, D. Kopf, K. Wiesauer, E. Breuer, and D. Stifter, "Supercontinuum generation system for optical coherence tomography based on tapered photonic crystal fibre," Opt. Express **14**(4), 1596–1603 (2006).

#185206 - $15.00 USD Received 11 Feb 2013; revised 3 Apr 2013; accepted 8 Apr 2013; published 26 Apr 2013

9. Y. Wang, Y. Zhao, J. S. Nelson, Z. Chen, and R. S. Windeler, "Ultrahigh-resolution optical coherence tomography by broadband continuum generation from a photonic crystal fiber," Opt. Lett. **28**(3), 182–184 (2003).
10. B. A. Cumberland, J. C. Travers, S. V. Popov, and J. R. Taylor, "29 W High power CW supercontinuum source," Opt. Express **16**(8), 5954–5962 (2008).
11. B. H. Chapman, J. C. Travers, S. V. Popov, A. Mussot, and A. Kudlinski, "Long wavelength extension of CW-pumped supercontinuum through soliton-dispersive wave interactions," Opt. Express **18**(24), 24729–24734 (2010).
12. W. J. Wadsworth, N. Joly, J. C. Knight, T. A. Birks, F. Biancalana, and P. St. J. Russell, "Supercontinuum and four-wave mixing with Q-switched pulses in endlessly single-mode photonic crystal fibres," Opt. Express **12**(2), 299–309 (2004).
13. A. Rulkov, M. Vyatkin, S. Popov, J. Taylor, and V. Gapontsev, "High brightness picosecond all-fiber generation in 525-1800nm range with picosecond Yb pumping," Opt. Express **13**(2), 377–381 (2005).
14. J. K. Ranka, R. S. Windeler, and A. J. Stentz, "Visible continuum generation in air-silica microstructure optical fibers with anomalous dispersion at 800 nm," Opt. Lett. **25**(1), 25–27 (2000).
15. P. St. J. Russell, "Photonic-crystal fibers," J. Lightwave Technol. **24**(12), 4729–4749 (2006).
16. J. M. Dudley, G. Genty, and S. Coen, "Supercontinuum generation in photonic crystal fiber," Rev. Mod. Phys. **78**(4), 1135–1184 (2006).
17. Heraeus Datasheet for Suprasil glass.
18. J. Troles, Y. Niu, C. Duverger-Arfuso, F. Smektala, L. Brilland, V. Nazabal, V. Moizan, F. Desevedavy, and P. Houizot, "Synthesis and characterization of chalcogenide glasses from the system Ga-Ge-Sb-S and preparation of a single-mode fiber at 1.55 μm," Mater. Res. Bull. **43**(4), 976–982 (2008).
19. R. Gattass, L. B. Shaw, V. Q. Nguyen, P. C. Pureza, I. D. Aggarwal, and J. S. Sanghera, "All-fiber chalcogenide-based mid-infrared supercontinuum source," Opt. Fiber Technol. **18**(5), 345–348 (2012).
20. D. D. Hudson, S. A. Dekker, E. C. Mägi, A. C. Judge, S. D. Jackson, E. B. Li, J. S. Sanghera, L. B. Shaw, I. D. Aggarwal, and B. J. Eggleton, "Octave spanning supercontinuum in an As_2S_3 taper using ultralow pump pulse energy," Opt. Lett. **36**(7), 1122–1124 (2011).
21. A. Marandi, C. W. Rudy, V. G. Plotnichenko, E. M. Dianov, K. L. Vodopyanov, and R. L. Byer, "Mid-infrared supercontinuum generation in tapered chalcogenide fiber for producing octave-spanning frequency comb around 3 μm," Opt. Express **20**(22), 24218–24225 (2012).
22. J. Troles, Q. Coulombier, G. Canat, M. Duhant, W. Renard, P. Toupin, L. Calvez, G. Renversez, F. Smektala, M. El Amraoui, J. L. Adam, T. Chartier, D. Mechin, and L. Brilland, "Low loss microstructured chalcogenide fibers for large non linear effects at 1995 nm," Opt. Express **18**(25), 26647–26654 (2010).
23. V. R. Almeida, R. R. Panepucci, and M. Lipson, "Nanotaper for compact mode conversion," Opt. Lett. **28**(15), 1302–1304 (2003).
24. F. Smektala, C. Quemard, V. Couderc, and A. Barthelemy, "Non-linear optical properties of chalcogenide glasses measured by Z-scan," J. Non-Cryst. Solids **274**(1-3), 232–237 (2000).
25. N. Granzow, S. P. Stark, M. A. Schmidt, A. S. Tverjanovich, L. Wondraczek, and P. St. J. Russell, "Supercontinuum generation in chalcogenide-silica step-index fibers," Opt. Express **19**(21), 21003–21010 (2011).
26. S. P. Stark, F. Biancalana, A. Podlipensky, and P. St. J. Russell, "Nonlinear wavelength conversion in photonic crystal fibers with three zero-dispersion points," Phys. Rev. A **83**, 023808 (2011).
27. M. Artiglia, G. Coppa, P. Di Vita, M. Potenza, and A. Sharma, "Mode field diameter measurements in single-mode optical fibers," J. Lightwave Technol. **7**(8), 1139–1152 (1989).
28. M. A. Foster, K. D. Moll, and A. L. Gaeta, "Optimal waveguide dimensions for nonlinear interactions," Opt. Express **12**(13), 2880–2887 (2004).
29. N. Granzow, P. Uebel, M. A. Schmidt, A. S. Tverjanovich, L. Wondraczek, and P. St. J. Russell, "Bandgap guidance in hybrid chalcogenide-silica photonic crystal fibers," Opt. Lett. **36**(13), 2432–2434 (2011).
30. H. W. Lee, M. A. Schmidt, R. F. Russell, N. Y. Joly, H. K. Tyagi, P. Uebel, and P. St. J. Russell, "Pressure-assisted melt-filling and optical characterization of Au nano-wires in microstructured fibers," Opt. Express **19**(13), 12180–12189 (2011).
31. D. Lezal, J. Pedlikova, J. Gurovic, and R. Vogt, "The preparation of chalcogenide glasses in chlorine reactive atmosphere," Ceramics-Silikaty **40**, 55–59 (1996).
32. M. F. Churbanov, I. V. Scripachev, G. E. Snopatin, V. S. Shiryaev, and V. G. Plotnichenko, "High-purity glasses based on arsenic chalcogenides," J. Optoelectron. Adv. Mater. **3**, 341–349 (2001).
33. N. Da, L. Wondraczek, M. A. Schmidt, N. Granzow, and P. St. J. Russell, "High index-contrast all-solid photonic crystal fibers by pressure-assisted melt infiltration of silica matrices," J. Non-Cryst. Solids **356**(35-36), 1829–1836 (2010).
34. J. Bethge, J. Jiang, C. Mohr, M. Fermann, and I. Hartl, "Optically Referenced Tm-Fiber-Laser Frequency Comb," in Lasers, Sources, and Related Photonic Devices, OSA Technical Digest (CD) (Optical Society of America, 2012), paper AT5A.3.
35. P. Kinsler, "Optical pulse propagation with minimal approximations," Phys. Rev. A **81**(1), 013819 (2010).
36. C. Xiong, E. Magi, F. Luan, A. Tuniz, S. Dekker, J. S. Sanghera, L. B. Shaw, I. D. Aggarwal, and B. J. Eggleton, "Characterization of picosecond pulse nonlinear propagation in chalcogenide As_2S_3 fiber," Appl. Opt. **48**(29), 5467–5474 (2009).

#185206 - $15.00 USD Received 11 Feb 2013; revised 3 Apr 2013; accepted 8 Apr 2013; published 26 Apr 2013

37. A. Tuniz, G. Brawley, D. J. Moss, and B. J. Eggleton, "Two-photon absorption effects on Raman gain in single mode As_2Se_3 chalcogenide glass fiber," Opt. Express **16**(22), 18524–18534 (2008).

1. Introduction

Supercontinuum (SC) light is useful in a large number of technical and scientific applications including spectroscopy [1,2], nonlinear microscopy [3,4], optical metrology [5], frequency comb generation [6] or optical coherence tomography [7–9]. It can be efficiently generated in a variety of different optical fibers pumped by both continuous wave and pulsed lasers [10–14]. SC generation relies on the interplay of nonlinear effects such as self-phase modulation, four-wave mixing, soliton dynamics and Raman scattering, and to be efficient it requires an optical waveguide with suitably designed group velocity dispersion (GVD), including a zero dispersion wavelength (ZDW) close to the pump wavelength. Solid-core photonic crystal fiber (PCF) is particularly interesting because it allows the ZDW to be adjusted over a wide spectral range [15,16]. PCF is most usually fabricated from fused silica glass, a material with low material attenuation in the visible and near infrared (IR) that is well suited to the fiber drawing process.

A major drawback of silica fibers is strong attenuation at vacuum wavelengths longer than $\lambda = 2$ µm, which limits SC generation to the near-IR [17]. Generating SC light in the mid-IR therefore requires new materials, especially for the core. Chalcogenide glasses are interesting candidates, combining as they do nonlinear refractive indices that are ~200 times greater than fused silica, high refractive indices and a transparency window that can extend out beyond $\lambda =$ 10 µm. A number of different waveguide structures based on chalcogenide glasses have been reported in literature, including step-index fibers [18,19], fiber tapers [20,21] and microstructured fibers [22].

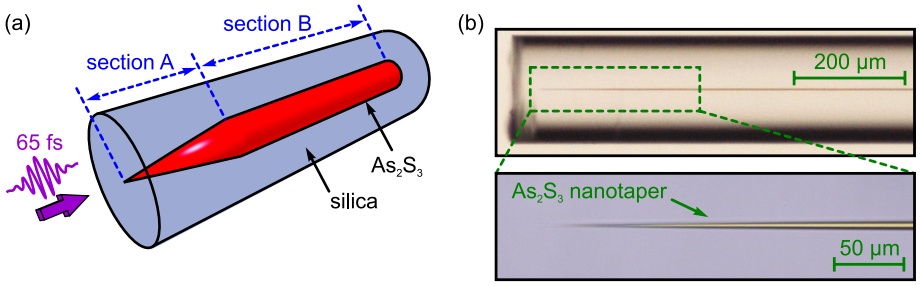

Fig. 1. (a) Schematic of the nano-spike chalcogenide-silica step-index waveguide. Section A shows the nano-spike used for efficient incoupling. The supercontinuum is generated in the constant-diameter part (section B). (b) Side images, taken with an optical microscope, of the waveguide used in the experiments. The core diameter increases from 0 to 1 µm along the 300 µm long taper transition.

In this paper we report efficient mid-IR SC-generation at extremely low pump pulse energies (< 20 pJ) in a hybrid step-index waveguide consisting of a cylindrical chalcogenide core embedded in a silica fiber capillary (Fig. 1(a)). At the input end the chalcogenide core is inversely tapered down to diameters below 100 nm, forming a 300 µm long "nano-spike", labeled section A in Fig. 1(a) (a similar device has previously been reported in the silicon-on-insulator system [23]). Adiabatic mode conversion along this spike increases the in-coupling efficiency of the 2 µm laser light into the sub-wavelength core by a factor of ~60. The core diameter in the 2-mm-long untapered section (labeled B in Fig. 1(a)) is kept constant at 1 µm, this being matched to the GVD requirements of the nonlinear processes. Upon launching ultrashort pulses from a Tm-doped fiber laser (65 fs pulses centered at λ ~2 µm) into the chalcogenide core, an octave-spanning SC, out to 4 µm, is obtained for input pulse energies as low as 18 pJ. Numerical simulations based on the generalized nonlinear Schrödinger equation agree well with the experimental results.

#185206 - $15.00 USD Received 11 Feb 2013; revised 3 Apr 2013; accepted 8 Apr 2013; published 26 Apr 2013

2. Fiber design

The core glass used is As_2S_3, (refractive index n_{co} = 2.43 at λ = 2 μm) and the cladding is fused silica (refractive index n_{cl} = 1.44 at λ = 2 μm), yielding a core-cladding index contrast $2(n_{co} - n_{cl})/(n_{co} + n_{cl})$ of 0.51 at the pump wavelength. This permits strong modal confinement in a small core, which together with a bulk nonlinearity that is ~250 times higher than silica [24] results in a γ coefficient of ~30 rad.$W^{-1}m^{-1}$, i.e., some 20,000 times greater than in standard single-mode (SM) telecommunications fiber. Efficient SC generation is achieved if the GVD is slightly anomalous and the ZDW not too distant from the pump wavelength [25,26]. These conditions are satisfied for a core diameter of 1 μm, resulting in a GVD of ~0.37 fs.$nm^{-1}mm^{-1}$ at λ = 2 μm (green curve in Fig. 2(a)), with a region of anomalous dispersion between λ = 1.35 μm and λ = 2.5 μm (magenta-colored area in Fig. 2(a)). The calculations were performed by directly solving Maxwell's equations in cylindrical coordinates and applying appropriate boundary conditions. The modal attenuation is less than 1 dB/mm over the whole range from λ = 1 μm to λ = 4 μm (Fig. 2(b)), being only 0.23 dB/m at λ = 2 μm. Beyond 4 μm it is dominated by the absorption of fused silica, which ultimately limits the SC bandwidth obtainable.

Efficient excitation of a guided mode with spatial FWHM less than λ/2 is impossible, even with the best lens and a numerical aperture (NA) of 1. The waveguide launching system used in our experiment has a NA of 0.21, yielding a minimum FWHM spot diameter at λ = 2 μm of ~6 μm. The FWHM modal diameter in section B is 918 nm, i.e., much smaller than 6 μm, so that only a fraction of the incoming light can couple into the core mode. The NA of the guided mode is 1.95 (grey dashed line in Fig. 3), which essentially means that at the fiber end-face a large fraction of the plane-wave spectrum is unable to radiate into air. Preliminary experiments for an untapered chalcogenide-silica waveguide with core diameter 1 μm gave launch efficiencies of just 0.2% at λ = 2 μm.

Up-tapering the core diameter at the input end is an option for improving the launch efficiency, but it has the major disadvantage (especially when the core-cladding index step is high) that the core becomes highly multimode (MM) and strong inter-modal coupling occurs in the taper. As a result the nonlinear broadening is highly irreproducible and extremely sensitive to external perturbations.

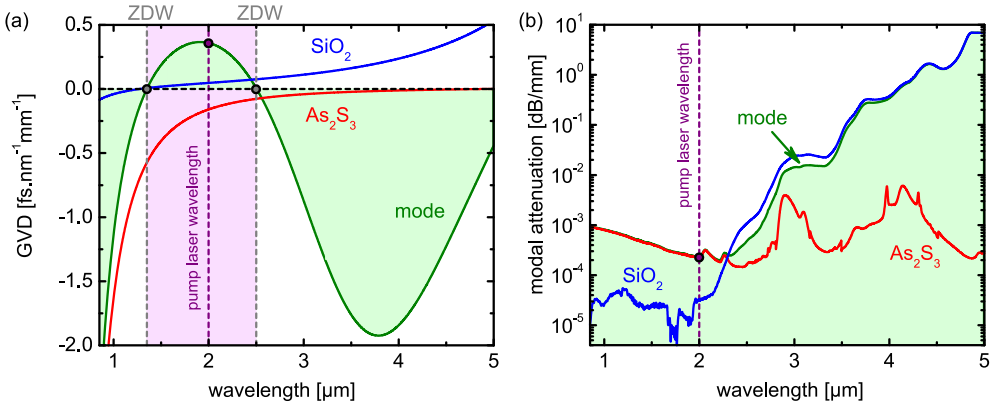

Fig. 2. (a) Group velocity dispersion of the fundamental mode of the chalcogenide-silica waveguide (core diameter 1 μm, section B in Fig. 1(a)). The wavelength of the pump laser (~2.0 μm, indicated by the purple dashed line) falls into the anomalous dispersion regime (magenta area). (b) Modal attenuation (green curve). For both diagrams, the red and the blue curves show the corresponding material properties of As_2S_3 and SiO_2.

To overcome poor launch efficiencies and multimode operation, we created an inverse-tapered launching "nano-spike" (section A in Fig. 1(a)). This spike allows the launch efficiency to be increased to 12%, some 60 times higher than in an untapered core. Along the

#185206 - $15.00 USD Received 11 Feb 2013; revised 3 Apr 2013; accepted 8 Apr 2013; published 26 Apr 2013

300-µm-long taper section, the core diameter increases from zero to 1 µm (the spatial resolution of the optical microscope was ~300 nm, meaning that the tip of the spike could not be resolved). Close to the tip of the spike, the core radius is much smaller than needed for single mode operation (the first higher order mode cuts in at a diameter of 782 nm, Fig. 3) and the mode extends out strongly into the silica (the mode field diameters were calculated using a published definition for non-Gaussian beam diameters [27, 28]). It is remarkable that for core diameters below 200 nm the mode spreads out more than 100 µm into the cladding. Indeed, the fraction of power flowing in the cladding depends strongly on the local taper diameter (red curves in Fig. 3), which in turn depends on the position along the spike, so that mode-matching can be achieved by moving the spike axially into the focus of the incoming beam. For a focal waist of 6 µm the optimum taper diameter is ~330 nm (the blue dot in Fig. 3). Since the mode extends strongly into the cladding for very narrow cores (red curves in Fig. 3), its field is almost entirely in the silica, which strongly reduces the Fresnel reflections that would occur at the input face of an untapered As_2S_3 core. If we assume a chalcogenide core diameter of 6 µm (which is the diameter giving the best modal overlap with respect to the input beam), the reflectivity at the fiber end-face would be 15.4% (bulk reflectivities of As_2S_3 and silica are 17.3% and 3.2%). When coupling light through the polished silica end-face of the device, however, the Fresnel reflection is almost identical to that of bulk silica, independent of the final core diameter. The spike reduces essentially to zero the Fresnel reflection at the As_2S_3-silica interfaces. We expect that the coupling efficiency can be improved with further optimization of the nanospike structure.

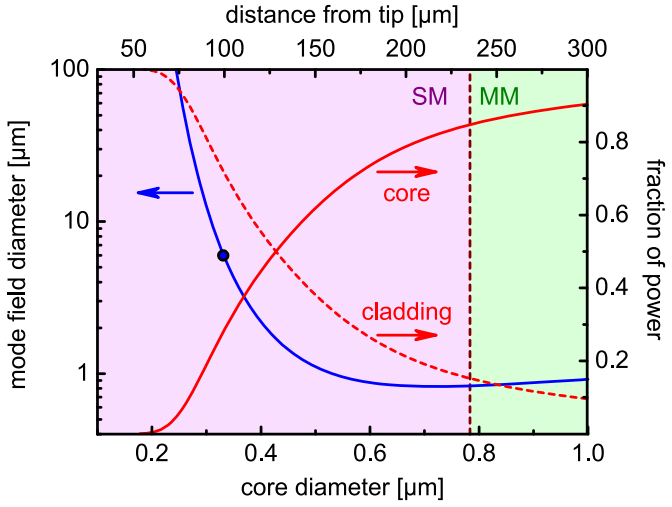

Fig. 3. Calculated mode field diameter (blue curve) as a function of local core diameter (the corresponding distance from the tip is given by the upper abscissa). The blue dot represents the core diameter and distance where the waist of the incoming beam matches the mode field diameter. The red curves represent the fractions of power flowing in core and cladding. SM and MM regions are indicated by the light red and green areas.

A significant advantage of the nano-spike, compared to a down-taper, is that the optimum core diameters lie in the single-mode regime. This allows clean excitation of the fundamental mode in a multimode waveguide, even if the core diameter lies significantly above the single-mode limit. When the core diameter reaches 1 µm, ~90% of the power is in the core. In the nano-spike the core contribution to the fiber nonlinearity, $\gamma^{co} = k_0 n_2^{co} / A_{eff}^{co}$ (k_0 is the vacuum wavevector, n_2^{co} the nonlinear refractive index of the core and A_{eff}^{co} the effective modal area), exceeds that of the cladding by some 3 orders of magnitude at any radius (red and blue curves in Fig. 4(a)). At λ = 2 µm the GVD is zero at core diameters of ~280 nm and ~840 nm

#185206 - $15.00 USD Received 11 Feb 2013; revised 3 Apr 2013; accepted 8 Apr 2013; published 26 Apr 2013

(indicated by yellow dots in Fig. 4(b)) with strong normal dispersion for diameters in between (grey curve in Fig. 4(a)). The regions of normal (orange-shaded area) and anomalous dispersion (grey-shaded area) calculated as a function of radius and wavelength are presented in Fig. 4(b).

3. Fabrication

The samples were fabricated by adapting the previously reported pressure-assisted melt filling technique, allowing the use of two materials that cannot be drawn together in a fiber pulling tower [24,29]. Instead of a furnace-based pressure cell, we used the spliced-fiber pressure-filling technique originally developed for producing gold-filled photonic crystal fibers [30]. A chalcogenide rod made of purified As_2S_3 (T_g = 198°C), with length 5 mm and diameter ~120 µm, was inserted into a silica capillary (inner diameter 150 µm, outer diameter 200 µm). The As_2S_3 purification procedure included melting arsenic and sulfur together with tellurium chlorides that act as a hydrogen getter [31]), followed by distillation of the chalcogenide melt, giving rise to a strong decrease of the O-H and S-H absorption bands located at 2.9 µm and 4.0 µm. The absorption at 4.0 µm was reduced from more than 100 dB/m (before purification) to 10 dB/m (after purification), corresponding to an impurity level of only 4 ppm [32].

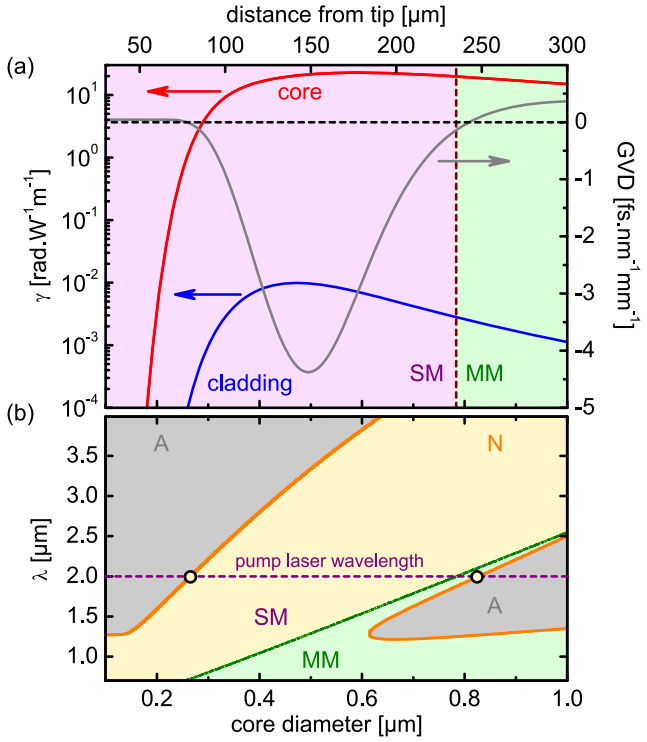

Fig. 4. (a) Contributions to the nonlinear coefficient of the guided mode from the core and the cladding (red: As_2S_3 core, blue: silica. All calculations were performed at λ = 2 µm). (b) Contour plot showing the regions of normal dispersion (yellow-shaded area) and anomalous dispersion (grey-shaded area) as a function of diameter and wavelength. The purple dashed line represents the pump laser of 2 µm. The waveguide is MM inside the green region and SM outside.

This capillary was fusion-spliced to a second silica capillary with the same outer diameter, but with a 1 µm wide central bore. The nanotaper was implemented by fusing shut one end of the capillary before filling. After heating the fiber to 600°C, pressurized argon was applied through the 150 µm capillary, forcing the chalcogenide melt into the 1 µm wide channel. Filling lengths of a few cm were routinely achieved for filling times of an hour. In all

#185206 - $15.00 USD Received 11 Feb 2013; revised 3 Apr 2013; accepted 8 Apr 2013; published 26 Apr 2013

experiments the chalcogenide strand showed bubbles and discontinuities along its entire length, which we attribute to out-gassing due to reboiling [33]. These bubbles were removed by flame-brushing the filled fiber, allowing us to produce cm-long chalcogenide strands continuous in both sections A and B (Fig. 1(b)). The filled fiber was cleaved off close to the end of the taper such that the tip remained fully encapsulated in the silica, protecting it from any environmental influences, in particular oxygen and water. The nanospike has the additional advantage of allowing the incoming light to be gently funneled into the chalcogenide core, reducing the risk of core damage. Previous experiments [29] have shown that the embedded chalcogenide glass has optical properties that are identical to those of the bulk material (advantageous for design and simulations) showing that there is no chemical interaction between the As_2S_3 and the silica. The technique requires only very small quantities of material (in contrast to fiber-drawing) and allows "problematic" core glasses to be used, e.g., glasses that cannot be drawn to fiber.

4. Optical set-up

Light from a Tm-doped fiber laser (λ = 2 µm, pulse duration 65 fs, repetition rate 100 MHz, pulse energy 3 nJ, average power 300 mW [34]) was launched into the nano-spike using an IR lens of focal length 4 mm (Fig. 5(a)). The incoupling was optimized by longitudinally moving the focus spot along the axis of the spike and searching for the location of maximum transmission, giving a maximum coupling efficiency of 12%. The output spectra were recorded using a Fourier transform infrared spectrometer (FTIR). Excitation of the fundamental mode was confirmed by projecting the output beam on to an IR mode profiler (output near field profile shown in the lower right-hand image of Fig. 5(b)).

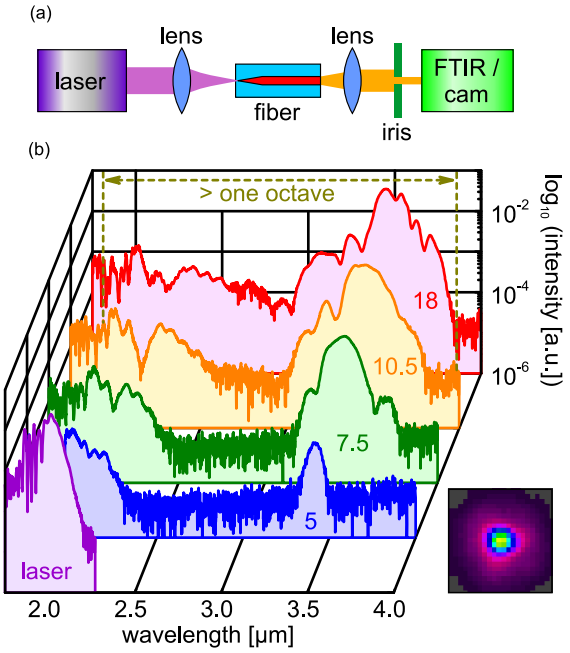

Fig. 5. (a) Schematic diagram of the SC set-up. Pulses from a Tm-doped fiber laser were coupled into the nano-spike using an IR lens. The transmitted light was recorded using an FTIR, after blocking any undesired cladding light using iris diaphragm. (b) Experimental SC spectra taken at different pulse energies (12% coupling efficiency, blue: 5.0 pJ, green: 7.5 pJ, orange: 10.5 pJ, red: 18 pJ). The purple curve represents the laser spectrum. The lower right-hand image shows the measured near-field profile of the mode at the output end of the waveguide.

#185206 - $15.00 USD Received 11 Feb 2013; revised 3 Apr 2013; accepted 8 Apr 2013; published 26 Apr 2013

5. Experimental results

Strong SC generation, spanning more than one octave and extending out to λ ~4 μm, was observed in sample lengths of only ~2 mm (Fig. 5b). The spectrum began to broaden at a pulse energy of 5 pJ, maximum broadening being achieved at only 18 pJ (this refers to the pulse energy in chalcogenide core, taking account of 12% coupling efficiency). We checked the stability of the SC over many hours on successive days by continuously launching pulses with energies of 18 pJ into the waveguide. It remained constant over time, showing no evidence of thermally-induced fluctuations or incoupling instabilities. Increasing the pulse energy did not produce a broader spectrum, which we attribute [25] to strong modal attenuation beyond 4 μm, where the loss reaches values of several dB/mm. Irreversible damage was seen in the nanotaper when the pulse energy exceeded 25 pJ.

If an untapered core is used, the very low launch efficiency (0.2%) strongly limits the spectral broadening.

6. Simulations

To simulate the generated output spectrum, we solve the unidirectional nonlinear field propagation equation [35]:

$$\frac{\partial A(z,\tau)}{\partial z} = DA(z,\tau) - i\left(\gamma(\omega_0) + i\gamma_1 \frac{\partial}{\partial \tau}\right) \times \left(A(z,\tau)\int_{-\infty}^{\infty} R(t')\left|A(z,\tau)\right|^2 dt'\right) \qquad (1)$$

using the split-step Fourier method. This equation describes the evolution of the pulse envelope during propagation along the nonlinear waveguide. The pulse envelope is $A(z,\tau)$, τ is the time in a reference frame moving at group velocity v_g ($\tau = t - z/v_g$) and t is the laboratory time. The dispersion and nonlinearity of the core mode are included via the operator D and the parameter $\gamma(\omega_0) = \gamma_0 + \gamma_1(\omega - \omega_0)$ with $\gamma_0 = 7.2\ \mathrm{W^{-1}m^{-1}}$ and $\gamma_1 = 7.68 \times 10^{-15}\ \mathrm{s.W^{-1}m^{-1}}$. We used a Raman response function with period 15.5 fs and coherence lifetime 230.5 fs [36,37].

The simulations show that the pulse, with parameters resembling those of a higher-order soliton, initially experiences self-compression, which causes broadening of the spectrum around the pump frequency. As a result of higher-order perturbations, the compressed soliton undergoes fission at a propagation distance of ~0.7 mm from the point of optimum incoupling (the blue dot in Fig. 3). At this point, dispersive waves are generated at both short and long wavelengths (~800 and ~3500 nm) in the regions of normal dispersion (see Fig. 2(a)). The pump wavelength itself is also shifted slightly towards longer wavelengths due to the Raman effect.

Simulations based on numerical solutions of Eq. (1) show that maximum spectral broadening is achieved after 1 mm of propagation, in good agreement with the experimental results – longer samples did not yield broader spectra. As a result the sample length was restricted to ~2 mm in all the experiments.

#185206 - $15.00 USD Received 11 Feb 2013; revised 3 Apr 2013; accepted 8 Apr 2013; published 26 Apr 2013

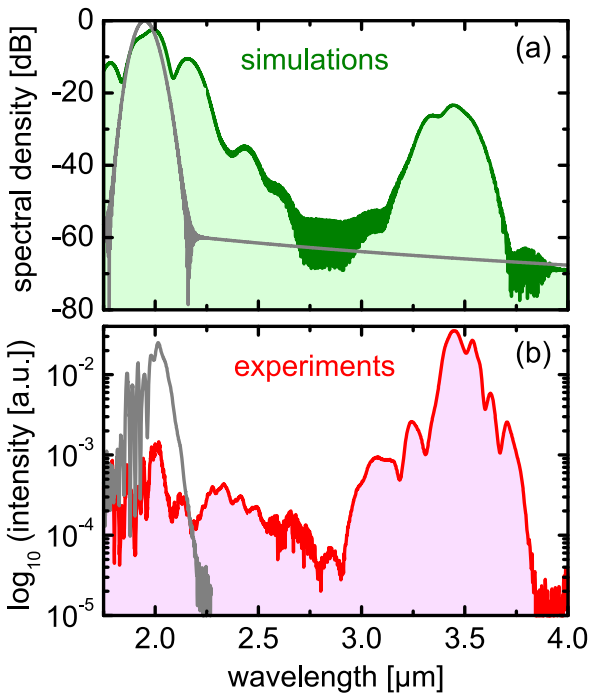

Fig. 6. Spectrum of the ultrashort optical pulse after propagating along the chalcogenide-silica waveguide (sample length 1.7 mm, including spike). (a) Numerical simulations. (b) Experimental results (parameters given in the text). In both diagrams the grey curve represents the input spectrum.

The simulated spectrum (Fig. 6(a)) agrees fairly well with the experimental results (Fig. 6(b)) except on the short wavelength side. We attribute this discrepancy to wavelength-dependent coupling of the output light into the spectrometer is (caused, e.g., by chromatic aberrations in the lenses). The simulations also show that the spike itself has no influence on the spectral properties of the output light, all the nonlinear effects occurring entirely inside the constant-diameter part of the structure (section A in Fig. 1(b)).

7. Conclusions

In conclusion, an efficient mid-IR SC can be generated using a new type of hybrid optical waveguide consisting of a highly nonlinear As_2S_3 core (core diameter 1 μm) and a silica cladding. At its input end the core is inversely tapered down to diameters below 200 nm. Due to the strong extension of the modal field into the silica cladding at very small core diameters, mode-matching to an incoming beam is possible, increasing the coupling efficiency by a factor of 60 compared to direct launching into a core with a flat (untapered) endface. An octave-spanning SC extending out to almost 4 μm was produced using fs pulses of only 18 pJ energy. The nano-spike approach provides a unique means of solving the long-standing problem of efficiently coupling light into single-mode high-index contrast waveguides of sub-wavelength diameter.

Acknowledgment

This work was partly funded by the German Science Foundation (DFG) via grants WO1220/4-2 and SCHM2655/1-2.

#185206 - $15.00 USD Received 11 Feb 2013; revised 3 Apr 2013; accepted 8 Apr 2013; published 26 Apr 2013